https://doi.org/10.5194/egusphere-2026-1047
Preprint. Discussion started: 6 March 2026

All-sky ATMS radiance data assimilation with MPAS-JEDI

Junmei Ban[1], Zhiquan Liu[1], Byoung-Joo Jung[1], Ivette Hernandez Banos[1],
Benjamin Ruston[2], and Andrew Collard[3]

[1]NSF National Center for Atmospheric Research, Boulder, Colorado, USA
[2]Joint Center for Satellite Data Assimilation, Boulder, Colorado, USA
[3]National Centers for Environmental Prediction, College Park, Maryland, USA

Correspondence to: Junmei Ban (jban@ucar.edu)

Abstract. This study extends the all-sky radiance data assimilation capability in MPAS-JEDI (data assimilation system for the Model for Prediction Across Scales-Atmosphere based upon the Joint Effort for Data assimilation Integration), previously implemented for the Advanced Microwave Sounding Unit-A (AMSU-A), to the Advanced Technology Microwave Sounder (ATMS). Compared with AMSU-A, ATMS covers a broad frequency range, including high-frequency humidity-sounding channels, in addition to the temperature-sounding and low-frequency imager channels. In contrast to the previous AMSU-A implementation, which assimilated only imaging channels under all-sky conditions, this work assimilates all ATMS channels using the all-sky approach. A situation-dependent observation error model is employed, with distinct cloud predictors over land and ocean surfaces for both temperature- and humidity-sounding channels. The analysis variables, radiance observation operator, and bias correction method are inherited from the AMSU-A all-sky assimilation. The impact of assimilating all-sky ATMS radiances is evaluated with three month-long global hybrid three-dimensional ensemble-variational (hybrid-3DEnVar) experiments: a benchmark experiment without ATMS data, an experiment assimilating only ATMS temperature-sounding channels, and an experiment assimilating all ATMS channels. The 6-hour background forecasts during the assimilation cycling and extended 5-day forecasts are verified against conventional observations, satellite radiances, and Global Forecast System (GFS) analysis. The results show that the background fits to radiosonde observations, satellite radiances, and GFS analyses have improved. Forecast verifications against GFS analyses and independent radiance observations demonstrate statistically significant improvements relative to the benchmark for up to 3 days in both ATMS experiments, across dynamic, thermodynamic, moisture, and cloud fields.

1 Introduction

Over the past decade, numerical weather prediction (NWP) centers have advanced in assimilating satellite radiance data from clear-sky conditions to all-weather conditions, i.e., all-sky radiance data assimilation (DA) (e.g., Geer et al., 2018). The European Centre for Medium-Range Weather Forecasts (ECMWF) initiated all-sky radiances DA from microwave imagers and humidity sounders, including the Special Sensor Microwave Imager (SSM/I), the Advanced Microwave Scanning Radiometer for the Earth Observing System (AMSR-E) (Bauer et al., 2010; Geer et al., 2010), and Microwave Humidity

Sounders (MHS) (Geer et al., 2014). Subsequently, the Global Precipitation Measurement (GPM) Microwave Imager (GMI) (Kazumori et al., 2016), MicroWave Humidity Sounder 2 (MWHS-2) (Lawrence et al., 2018), and Advanced Microwave Sounding Unit-A (AMSU-A) (Duncan et al., 2022a) have also been assimilated using the all-sky approach. Geer et al. (2017) highlighted the significant positive impacts of all-sky assimilation of microwave imagers and humidity sounders on medium-range forecasts. Assimilating temperature-sounding channels under all-sky conditions presents greater challenges. As noted by Geer et al. (2018) and Weston et al. (2019), these challenges arise from (1) poor quality of scattering simulations at the 50 GHz frequencies of these instruments (such as AMSU-A), (2) smaller temperature background errors compared to humidity background errors, and (3) the more non-linear response of microwave temperature-sounding observations to cloud and precipitation compared with humidity-sounding observations. The development of AMSU-A temperature-sounding channel assimilation has progressed from incorporating only channels 4 and 5 over the ocean (Geer et al., 2012) to assimilate all temperature-sounding channels (channels 5 and above) over both ocean and land (Weston et al., 2019; Duncan et al., 2022b). The improvements in all-sky assimilation have also benefited from enhancements in the forecast model, the radiative transfer model (Bauer et al., 2006; Geer et al., 2009), and situation-dependent observation-error models (Geer and Bauer 2011).

At the National Centers for Environmental Prediction (NCEP), cloudy radiances from the AMSU-A and Advanced Technology Microwave Sounder (ATMS) over ocean are assimilated in the Global Forecast System (GFS) using the Gridpoint Statistical Interpolation (GSI) analysis system (Zhu et al., 2016, Zhu et al., 2019). Earlier limitations in the cloud microphysics parameterization of the original Global Spectral Model (GSM)-based GFS (Zhao and Carr, 1997) prevented the assimilation of precipitation-affected radiances in the operational GFS Global Data Assimilation System (GDAS). At the UK Met Office, Migliorini and Candy (2019) and Candy and Migliorini (2021) demonstrated the benefits of all-sky assimilation of AMSU-A and MHS, respectively. For AMSU-A, the progress began with temperature-sounding channels (channel 4 and 5 from AMSU-A) over ocean, excluding precipitation scenes.

The ATMS is a cross-track microwave radiometer onboard the Suomi National Polar-orbiting Partnership (SNPP) satellite, launched in October 2011 and NOAA-20/21 (N20; N21), launched in November 2017 and 2022, respectively. It has 22 channels, including low-frequency imager channels, temperature-sounding channels (~ 50 GHz), and high-frequency humidity-sounding channels (~ 183 GHz). At NCEP, operational assimilation of non-precipitating cloudy ATMS radiances over the ocean began in 2019 (Zhu et al., 2019), with mostly neutral impact. Tong et al. (2020) extended GSI to assimilate precipitation-affected radiances by using a more advanced microphysics scheme, demonstrating neutral to positive impact on overall forecast skill. At ECMWF, clear-sky ATMS DA has been operationally assimilated since September 2012 (Bormann et al., 2013), with further improvements by accounting for inter-channel error correlations and tuning error variances (Weston and Bormann, 2018). At Japan Meteorological Agency, clear-sky ATMS data have been assimilated operationally since 2017 (Murata and Kamekawa, 2019).

MPAS-JEDI, the data assimilation system for the Model for Prediction Across Scales-Atmosphere (MPAS; Skamarock et al., 2012) based on the Joint Effort for Data assimilation Integration (JEDI; Trémolet and Auligné, 2020) framework, was introduced by Liu et al. (2022). The system includes several algorithms, such as the three-dimensional variational (3DVar)

https://doi.org/10.5194/egusphere-2026-1047
Preprint. Discussion started: 6 March 2026

method, 3D/4D ensemble-variational (EnVar) method and their hybrid variants, ensemble of data assimilations (EDA), and EnKF-based methods (Liu et al., 2022; Guerrette et al., 2023; Jung et al., 2024; Nystrom et al., 2025; Sun et al., 2025). Liu et al. (2022) implemented all-sky radiance DA for AMSU-A window channels (1-4 and 15) within MPAS-JEDI's EnVar, demonstrating positive impacts. More recently, Sun et al. (2025) and Nystrom et al. (2025) showed the positive impact of all-sky AMSU-A radiances with MPAS-JEDI's LGETKF (gain form of the local ensemble transform Kalman filter) and hybrid-4DEnVar, respectively. In this study, we focus on ATMS all-sky assimilation, extending the previously implemented AMSU-A all-sky assimilation within MPAS-JEDI (Liu et al., 2022; Sun et al., 2025; Nystrom et al., 2025). Unlike AMSU-A, where temperature-sounding channels were assimilated under clear-sky conditions and only window channels were assimilated under all-sky conditions, we assimilate all ATMS temperature-sounding, humidity-sounding, and window channels using the all-sky approach. The outline of the paper is as follows. Section 2 describes ATMS observations. Section 3 details the all-sky data assimilation approach, including the observation error model, quality control, and the variational bias correction (VarBC). Section 4 presents the experimental design, and Section 5 and Section 6 provide the results and conclusions, respectively.

2 Observations

2.1 ATMS

ATMS integrates the capabilities of AMSU-A and MHS, offering higher spatial resolution and improved calibration accuracy (Weng et al., 2013). ATMS has a swath width of 2,600 km, exceeding that of AMSU-A (2,343 km), thereby achieving near-continuous spatial coverage at the equator. A comparison of the channel characteristics of ATMS with those of AMSU-A and MHS is presented in Table 1. Channels 1–2 and 16–17 are atmospheric window channels. These channels provide essential information on water vapor, cloud water, and surface emissivity. Channels 3–15 are situated within the oxygen absorption band (50–60 GHz) and closely match the AMSU-A channels, except for channel 4, which is a new addition in ATMS. High-peaking temperature sounding channels 11 to 15 are not used in this study considering the model top is at 30 km altitude (section 4). Channels 18–22 are located near a water vapor absorption band at 183 GHz, similar to MHS, but with two additional channels 19 and 21, to enhance moisture sounding. The ATMS observations from SNPP and N20 are used in this study. The data were obtained from the National Aeronautics and Space Administration Goddard Earth Sciences Data and Information Services Center (GES DISC). The original files are provided in HDF format and were converted to a format readable by JEDI Interface for Observation Data Access (IODA).

Table 1 ATMS channel information, with AMSU-A and MHS listed for reference. The channels in gray color are not assimilated in this study.

Channel	Freq.(GHz)	Channel	Freq.(GHz)
AMSU-A 1	23.8	ATMS 1	23.8
AMSU-A 2	31.4	ATMS 2	31.4

AMSU-A 3	50.3	ATMS 3	50.3
		ATMS 4	51.76
AMSU-A 4	52.8	ATMS 5	52.8
AMSU-A 5	53.596	ATMS 6	53.596
AMSU-A 6	54.4	ATMS 7	54.4
AMSU-A 7	54.94	ATMS 8	54.94
AMSU-A 8	55.5	ATMS 9	55.5
AMSU-A 9	fo=57.29	ATMS 10	fo=57.29
AMSU-A 10	fo±0.217	ATMS 11	fo±0.217
AMSU-A 11	fo±0.3222±0.048	ATMS 12	fo±0.3222±0.048
AMSU-A 12	fo±0.3222±0.022	ATMS 13	fo±0.3222±0.022
AMSU-A 13	fo±0.3222±0.010	ATMS 14	fo±0.3222±0.010
AMSU-A 14	fo±0.3222±0.045	ATMS 15	fo±0.3222±0.045
AMSU-A 15	89.0	ATMS 16	88.2
MHS 1	89.0		
MHS 2	157.0	ATMS 17	165.5
MHS 5	183.31±7.0	ATMS 18	183.31±7.0
		ATMS 19	183.31±4.5
MHS 4	183.31±3.0	ATMS 20	183.31±3.0
		ATMS 21	183.31±1.8
MHS 3	183.31±1.0	ATMS 22	183.31±1.0

2.2 Other observations

This study assimilates non-radiance observations, including radiosondes, aircraft data, Global Navigation Satellite System Radio Occultation (GNSSRO) bending angles, atmospheric motion vectors, and surface pressure. In addition, radiance observations from AMSU-A (on NOAA-15/18/19, METOP-A/B, and Aqua) and MHS (on NOAA-18/19 and METOP-A/B) are also assimilated. Radiance and non-radiance datasets are provided in NCEP's BUFR and PREPBUFR formats, respectively, and were obtained from the NCAR Research Data Archive (RDA) archived GDAS. The exception is MHS data, which were sourced from GSI's NCDIAG files and pre-quality controlled, following the procedure described by Liu et al. (2022). All data were converted to the IODA format prior to assimilation.

The independent radiance data from the Global Precipitation Measurement Mission (GPM) Microwave Imager (GMI) and the Advanced Baseline Imager (ABI) onboard the GOES-16 geostationary platform are used to verify forecast performance. GMI (Draper et al., 2015) is a conically scanning microwave radiometer with 13 channels, covering frequencies from 10 GHz to 183 GHz. Its swath width is approximately 885 km, and the field of view ranges from 5 to 25 km depending on frequency. The GMI Level 1B data used in this study were obtained from the Japan Aerospace and Exploration Agency (JAXA). For GOES-

16 ABI, the full-disk radiance data is centered at 75.2° west longitude. There are 16 total channels, six of which are sensitive to liquid and solid phase water in clouds, e.g., water vapor channels 8, 9, and 10 and window channels 13, 14, and 15.

3 The all-sky data assimilation approach

The development of cloud and moist-physics parameterizations, together with improvements in the radiative transfer model, has a significant impact on all-sky radiance assimilation. In addition, the observation error model, variational bias correction, and quality control procedures are also critical components, and their implementations vary among numerical NWP centers.

3.1 Radiative transfer model

Community Radiative Transfer Model (CRTM; Han et al. 2006) (version 2.3.0), developed at Joint Center for Satellite Data Assimilation (JCSDA), is used as the radiance observation operator. The advanced doubling-adding (ADA) method (Liu and Weng, 2006) is applied to solve the radiative transfer equation under scattering conditions. Scattering lookup tables provided in CRTM are generated using Mie-Lorenz theory, assuming spherical particles for both liquid and frozen hydrometeors. For fast computations of ocean reflectivity or emissivity, the Fast Microwave Emissivity Model (FASTEM-6, English and Hewison, 1998; Liu et al., 2010; Bormann et al., 2012; Kazumori and English, 2015) is employed. CRTM clear-sky simulations require vertical profiles of atmospheric temperature and water vapor, surface parameters (e.g., surface temperature and wind speed), and sensor geometry information as input. Cloudy-radiance simulations additionally require profiles of hydrometeor mixing ratios, effective radii, and cloud fraction. Model-level hydrometeor mixing ratios are converted into layer water paths for input into CRTM. The K-matrix routine of CRTM is used to compute brightness temperatures and their Jacobians with respect to temperature, moisture, and hydrometeor input variables.

3.2 Microphysics and hydrometeor input

A detailed description of the MPAS model can be found in Skamarock et al. (2012, 2018). This section focuses on the microphysics scheme. In this study, the WSM6 microphysics scheme (Hong and Lim, 2006) is employed, which includes five hydrometeor types: cloud liquid water, cloud ice, rainwater, snow, and graupel. For cloudy-radiance simulations, CRTM additionally requires cloud fraction and cloud effective radius as inputs, although these fields are not treated as analysis variables. For cloud fraction, we use the diagnosed output from the MPAS model forecast, following the approach of Xu and Randall (1996). The cloud effective radius is defined as the ratio of the third to the second moment of a given particle size distribution (PSD),

$$R_e = \frac{\int_0^\infty r^3 n(r)dr}{\int_0^\infty r^2 n(r)dr}, \qquad (1)$$

where r is the particle radius, and $n(r)$ is the PSD. For the WSM6 scheme, cloud water and cloud ice follow monodisperse distribution, whereas rainwater, snow, and graupel follow exponential distribution. With the definition of effective radius and the given PSDs, analytical formulae for R_e can be derived. The MPAS model internally calculates the effective radii of cloud liquid water, cloud ice, and snow to feed to the model's radiation scheme. Therefore, we directly utilize R_e values of these three hydrometeors from the MPAS-model's forecast output. The R_e calculation for rainwater and graupel within MPAS-JEDI following:

$$Re = \frac{1.5}{\lambda}, \tag{2}$$

where the slope parameter λ is defined as:

$$\lambda = \left(\frac{\pi \rho_{(r,g)} N_{(r,g)0}}{\rho q_{(r,g)}}\right)^{1/4}, \tag{3}$$

Here, ρ refers to the dry air density in $kg\ \mathrm{m}^{-3}$, $q_{(r,g)}$ is the mixing ratio ($kg\ kg^{-1}$) of rainwater or graupel. For rainwater, the density $\rho_r = 1 \times 10^3\ \ kg\ \mathrm{m}^{-3}$, and the intercept parameter is $N_{r0} = 8 \times 10^6\ \mathrm{m}^{-4}$. For graupel, $\rho_g = 5 \times 10^2\ \ kg\ \mathrm{m}^{-3}$, $N_{x0} = 4 \times 10^6\ \mathrm{m}^{-4}$.

3.3 Situation-dependent observation error model

The situation-dependent observation error model is originally proposed by Geer and Bauer (2011). In MPAS-JEDI, for the clear-sky approach, a constant observation error is assigned to each individual channel of a satellite instrument. For radiance assimilation using the all-sky approach, situation-dependent observation error model is applied.

For ATMS over the ocean, same as Zhu et al. (2016), the Cloud Liquid Water (CLW) is retrieved following Grody et al. (2001).

$$CLW\ = cos\theta\{c_0 + c_1 ln[285 - T_b(1)] + c_2 ln[285 - T_b(2)]\} \tag{4}$$

where, $c_0 = 8.240 - (2.622 - 1.846cos\theta)cos\theta$, $c_1 = 0.754\ kg\ (m^2K)^{-1}$, $c_2 = -2.265\ kg\ (m^2K)^{-1}$. Here, θ is the zenith angle, and $T_b(1)$ and $T_b(2)$ are the brightness temperatures for ATMS channels 1 and 2, respectively. The CLW is computed from the observation CLW_{obs} and the first guess CLW_{fg}. The symmetric cloud amount predictor $\overline{CLW}$ is the average of CLW_{obs} and CLW_{fg},

$$\overline{CLW}\ = (CLW_{obs} + CLW_{fg})/2 \tag{5}$$

Follow Geer and Bauer (2011), the observation error σ_0 is assigned as a piecewise-linear ramp function of symmetric cloud metric,

$$\sigma_0 = \begin{cases} \sigma_0^{clr}\ , & if\ \overline{CLW}\ \le C_{clr} \\ \sigma_0^{clr} + \lambda(\overline{CLW} - C_{clr})\ , & if\ C_{clr} < \overline{CLW}\ \le C_{cld}\ , \\ \sigma_0^{cld}, & if\ \overline{CLW}\ \ge C_{cld} \end{cases} \tag{6}$$

with

$$\lambda = \frac{\sigma_0^{cld} - \sigma_0^{clr}}{C_{cld} - C_{clr}}, \tag{7}$$

C_{cld} and C_{clr} are the two cloud thresholds, and σ_0^{clr} and σ_0^{cld} are the minimum and maximum errors associated with C_{clr} and C_{cld}.

Over land, we follow the method proposed by Geer et al. (2014), who used a scattering index derived from 90 GHz and 150 GHz for all-sky assimilation of the three water vapor channels of MHS. In this study, we select 88.2 GHz (channel 16) and 165.5 GHz (channel 17) as the cloud predictor for both temperature and humidity sounding channels. A quadratic error model is applied over land.

$$SI = TB16 - TB17 \,, \tag{8}$$

where $TB16$ and $TB17$ are the brightness temperature of ATMS channel 16 and 17, respectively. The symmetric cloud amount is defined as the average of the observed and simulated cloud amounts:

$$\overline{SI} = (SI_{obs} + SI_{fg})/2 \,, \tag{9}$$

and the observation error is expressed as a quadratic function of the symmetric cloud amounts:

$$\sigma^0 = \begin{cases} \sigma_0^{clr} \,, \ if \ \overline{SI} \le C_{clr} \\ \sigma_0^{clr} + \lambda(\overline{SI} - C_{clr})^2 \,, \ if \ C_{clr} < \overline{SI} \le C_{cld} \\ \sigma_0^{cld} , \ if \ \overline{SI} \ge C_{cld} \end{cases} , \tag{10}$$

where

$$\lambda = \frac{\sigma_0^{cld} - \sigma_0^{clr}}{(C_{cld} - C_{clr})^2} \,, \tag{11}$$

The values used for the observation-error model are summarized in Table 2. The σ_0^{cld} values over the ocean used in this study are generally larger than those provided by Zhu et al. (2019), who assimilated AMTS cloudy radiances and excluded radiances affected by precipitation over the ocean. For channels 9 and 10, constant observation-error values are applied, as these channels are largely unaffected by clouds, and the all-sky error model is not applied.

Table 2 Parameters of the observation error model for NOAA20 ATMS channel 1-10 and 16-22.

Channel	Ocean				Land			
	C_{clr} $(kg\ m^{-2})$	C_{cld} $(kg\ m^{-2})$	σ_0^{clr} (K)	σ_0^{cld} (K)	C_{clr} (K)	C_{cld} (K)	σ_0^{clr} (K)	σ_0^{cld} (K)
1	0.03	0.53	4.40	35.23	not assimilated			
2	0.03	0.47	3.37	42.77	not assimilated			
3	0.03	0.41	2.56	17.89	not assimilated			
4	0.03	0.41	1.44	9.71	not assimilated			
5	0.03	0.43	0.53	4.33	not assimilated			
6	0.04	0.92	0.32	2.57	0.12	24.53	1.32	4.30
7	0.04	0.92	0.28	0.78	0.12	28.58	0.38	2.00
8	0.04	0.150	0.26	0.34	0.12	26.76	0.29	1.00
9	/	/	0.40	/	/	/	0.33	/
10	/	/	0.48	/	/	/	0.48	/

16	0.03	0.31	5.96	20.35	not assimilated			
17	0.03	0.53	2.88	35.56	not assimilated			
18	0.04	0.70	2.31	27.01	not assimilated			
19	0.04	0.70	2.21	20.55	0.12	25.99	4.23	26.32
20	0.04	0.70	2.31	17.50	0.12	24.87	3.64	23.27
21	0.04	0.70	2.53	13.15	0.12	29.56	3.32	20.66
22	0.04	0.70	2.81	9.92	0.12	27.64	3.17	16.80

Figure 1 shows the observation error model and standard deviation of observation-minus-background (OMB) for ATMS channel 19. When the averaged CLW is 0.04 $kg\ \mathrm{m}^{-2}$, both model and observations are considered cloud-free, resulting in a standard deviation of approximately 2.21 K. The standard deviation of the first-guess departures increases with CLW, and the linear fit captures the error growth between clear- and cloudy-sky conditions. Around CLW = 0.7 $kg\ \mathrm{m}^{-2}$, the standard deviation reaches a peak. For very high CLW values (averaged CLW > 1.5 $kg\ \mathrm{m}^{-2}$), large fluctuations in standard deviation are observed, which result from the limited number of available observations in these situations.

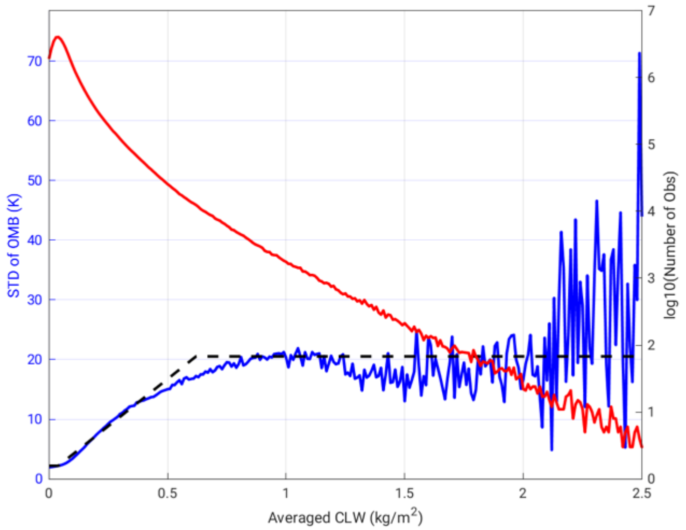

Figure 1 Observation error model (black dashed line) and standard deviation of OMB (blue curve) for ATMS channel 19 over water. The number of ATMS observations is shown in red curve. Statistics are computed over the period from 00 UTC 18 April to 18 UTC 14 May 2018 with a 6-h interval. The bin width for averaged CLW is $0.01\ kg\ \mathrm{m}^{-2}$.

https://doi.org/10.5194/egusphere-2026-1047
Preprint. Discussion started: 6 March 2026

3.4 Quality control

For non-radiance observations and AMSU-A, the quality control procedures are described in Sun et al. (2025). For ATMS, window channels and low-level sounding channels (1–5, 16, and 17) are assimilated over the ocean between 60°S and 60°N; in addition, channel 18 is assimilated over ocean only. Channels whose weighting functions extend above the 30-km model top are not assimilated. Following Zhu et al. (2016), topography check and situation-dependent check are used to inflate observation errors during ATMS assimilation. In the gross check, ATMS observations with absolute first-guess departures exceeding three times the final observation error are discarded. Finally, data thinning is applied to ATMS radiances using a 145-km thinning mesh.

3.5 VarBC

In MPAS-JEDI, the VarBC approach for all-sky microwave radiances is the same as for clear-sky radiances. Follow Zhu et al. (2014), in VarBC, the bias of a given observation is estimated using a linear predictor model based on a number of predefined predictors and the corresponding bias parameters, which are estimated together with the model state by including a bias term in the cost function of the variational analysis. The bias predictors include the constant offset; the temperature lapse rate and its square (both convolved with the channel's local response function based on the local transmittance profile); the emissivity Jacobian; and scan angle terms of the first, second, third, and fourth power. The bias correction coefficients are updated across the DA cycles.

4 Experimental design

MPAS-A is a non-hydrostatic model discretized on an unstructured centroidal Voronoi mesh in the horizontal with C-grid staggering of the state variables, and it can be configured for both global and regional applications (Skamarock et al., 2012, 2018). Same as Liu et al. (2022), Guerrette et al. (2023), and Jung et al. (2024), MPAS-A version 7.1 is used in this study. All experiments are conducted on a global quasi-uniform 60 km mesh (163,842 horizontal grid cells) low-resolution increments and ensemble inputs, and a 30 km mesh (655,362 grid cells) for high-resolution analysis. The model top is 30 km (~ 12 hPa) with 55 vertical levels. A time step of 180 s is used for the 30 km mesh. The "mesoscale reference" physics suite is employed, with detailed descriptions provided in Table 2 of Liu et al. (2022).

The dual-resolution (30km-60km) hybrid-3DEnVar is used, with a 25% weight in the static background error covariance (BEC) and a 75% weight in the ensemble BEC for non-cloud analysis variables. Static BEC for hydrometeors is not available at this time and thus 100% weight is given to the ensemble BEC for hydrometeor analysis variables when assimilating all-sky radiance data. The hybrid-3DEnVar uses an 80-member EDA ensembles at 60 km mesh. The standard deviation of static BEC is scaled to ⅓ of their actual statistics from the NMC method, and horizontal and vertical localization length scales are set to be 1200 km and 6 km, respectively.

Three month-long cycling experiments (Table 3) were conducted using MPAS-JEDI version 2.1.0, beginning at 0000 UTC 15 April 2018 and ending at 1800 UTC 14 May 2018. The benchmark experiment assimilates non-radiance observations and radiances from AMSU-A and MHS. Based on the benchmark, the ATMS_Tch experiment additionally assimilates ATMS temperature sounding channels 6-10 using the all-sky approach. The ATMS_THSch experiment further assimilates channels 1-5 and water vapor channels 18-22 and. 5-day extended forecasts were conducted at each 00 UTC initialization time.

Table 3. Hybrid-3DEnVar experiments

Experiments	Assimilated Observations
benchmark	Assimilated non-radiance data: radiosondes, aircraft, GNSSRO bending angle, atmospheric motion vectors, surface pressure. Radiances from AMSU-A and MHS: Clear-sky AMSU-A from NOAA-15 (channel 5, 7, 8, 9), NOAA-18 (channel 5, 6, 7, 8, 9), NOAA-19 (channel 5, 6, 7, 9), METOP-A (channel 5, 6, 9), METOP-B (channel 8, 9), Aqua (channel 8, 9) All-sky AMSU-A over water from NOAA-15/18/19, METOP-A (channel 1-4, and 15), METOP-B (channel 1-4) Clear-sky MHS from NOAA-18/19, METOP-A/B (channel 3-5)
ATMS_Tch	Same as benchmark, added ATMS channel 6-10 over both land and water.
ATMS_THSch	Same as ATMS_Tch, added (1) ATMS channel 18-22 which sensitive to humidity over both land and ocean, except channel 18 only over water. (2) ATMS channel 1-5 over ocean between 60°S and 60°N.

5 Results

In this section, the background (6-h forecast) is evaluated against radiosonde, AMSU-A, and MHS observations for the three experiments. For 5-day forecasts, the independent observations (i.e., not assimilated) from ABI and GMI are used for verification. GFS analyses are used in model space verification for both the background and 5-day forecasts.

5.1 Impact on the background

First, we evaluated the impact of ATMS assimilation on the virtual temperature (Tv), U and V wind components, and specific humidity (qv) profiles from radiosonde observations. Figure 2 presents the relative differences in 6-h forecast root mean square

https://doi.org/10.5194/egusphere-2026-1047
Preprint. Discussion started: 6 March 2026

error (RMSE) of ATMS_Tch and ATMS_THSch compared to the benchmark experiment. For Tv, ATMS_Tch exhibits an overall ~2% reduction in RMSE between 50°S and 50°N, with particularly notable improvements in the Northern Hemisphere. Since radiosonde observations are primarily concentrated in the Northern Hemisphere and sparsely distributed at high latitudes, the apparent degradation over the southern high latitudes is likely due to insufficient sample size for reliable statistics. Duncan et al. (2022b) reported temperature improvement mainly between 200 hPa and 300 hPa from radiosonde fits after assimilating all-sky AMSU-A temperature sounding channels. Similarly, in ATMS_Tch, small but statistically significant improvements in Tv are found around 250 hPa in the Northern Hemisphere. In contrast, ATMS_THSch shows a degradation in Tv around 10°S–10°N below 700 hPa (Fig. 2c). However, the corresponding standard deviation (not shown) indicates improvements in the same region, suggesting that the increased RMSE may primarily caused by a larger bias. For the wind field (Figs. 2d–2i), the benchmark experiment shows RMSE values exceeding 5 m s^{-1} for radiosonde U-wind observations in the tropical region above 100 hPa. Both ATMS_Tch and ATMS_THSch experiments demonstrate significant improvements in this region, largely attributed to the assimilation of ATMS channels 9 and 10, whose weighting function peaks are located near 200 hPa and 100 hPa, respectively. For specific humidity (Figs. 2j–2l), the benchmark experiment exhibits large RMSEs in the tropical lower troposphere (below 700 hPa). The ATMS_THSch experiment provides additional improvements beyond those achieved by ATMS_Tch. Liu et al. (2022, Fig. 3) reported that assimilating all-sky AMSU-A window channels yielded limited improvements in Tv, with the main benefits observed in the wind and specific humidity fields. Overall, the improved background fits to radiosondes after assimilating ATMS radiances are consistent with the findings of Liu et al. (2022), despite differences in the data assimilation algorithm and the set of assimilated observations.

https://doi.org/10.5194/egusphere-2026-1047
Preprint. Discussion started: 6 March 2026

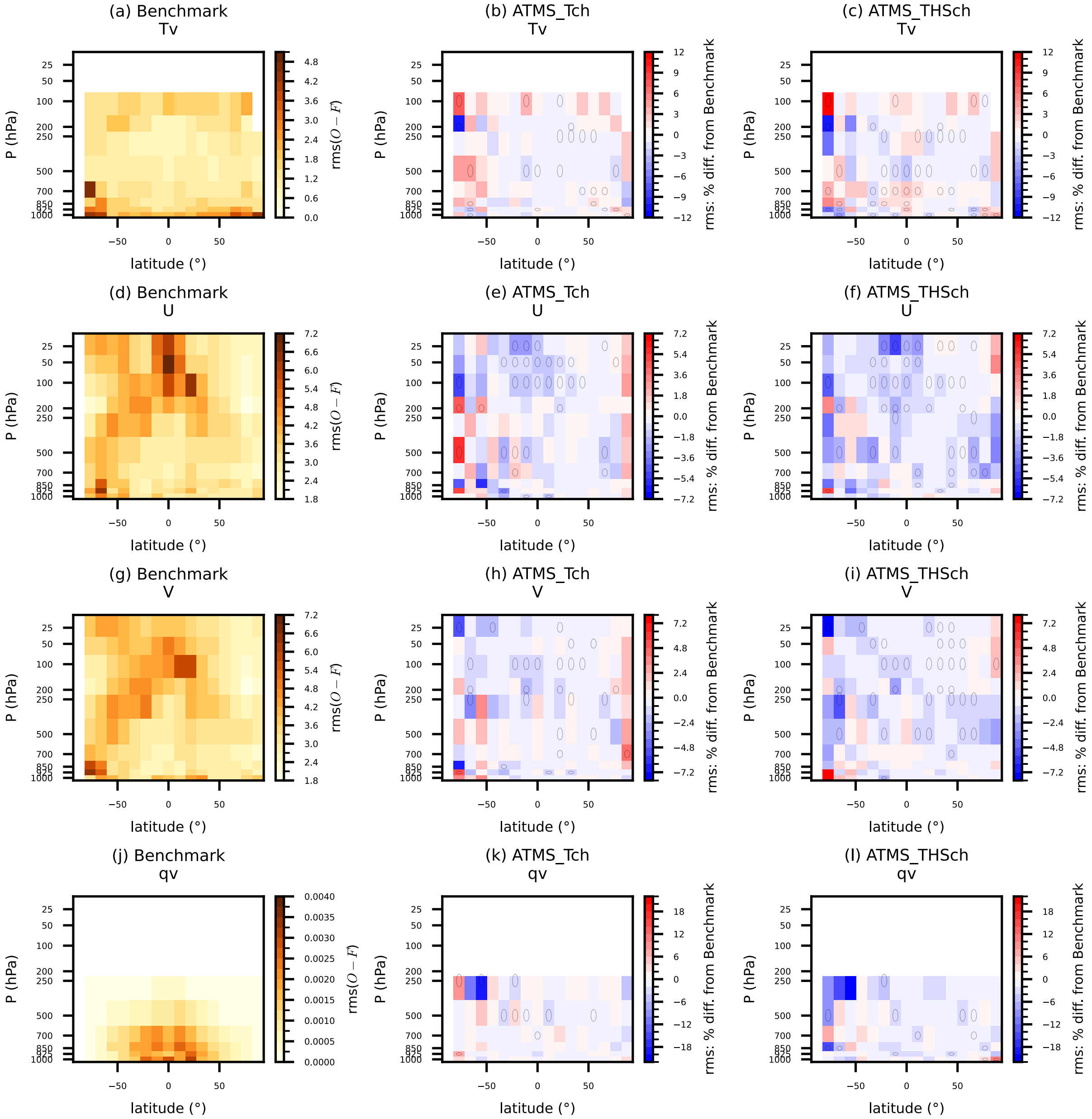

Figure 2. Left column: RMSE of 6-hr forecast from the benchmark experiment with respect to radiosondes Tv, U, V, and qv, respectively. Middle and right columns: relative RMSE difference (%) with respect to the RMSE of the benchmark for the ATMS_Tch and ATMS_THSch experiment. Positive values (red shading) indicate degraded fits, while negative values (blue shading) indicate improved fits relative to the benchmark. Statistics are aggregated over the period from 0000 UTC 18 April to 1800 UTC 14 May 2018. Light circles (middle/right columns) indicate latitude-level bins where differences are statistically significant. Latitude bins are spaced every 10°.

The 6-hour forecast background was further evaluated using satellite radiances. Figure 3 presents the latitudinal variation of relative RMSE reduction for METOP-A AMSU-A channels 4 and 15 brightness temperatures over the cycling period. A negative percentage indicates a positive impact from the ATMS_Tch and ATMS_THSch experiments relative to the benchmark. AMSU-A channel 4 (52.8 GHz) is primarily sensitive to cloud liquid water and temperature, with a smaller contribution from water vapor, while channel 15 (89.0 GHz), which peaks near the surface, is influenced by non-precipitating warm clouds in the lower atmosphere. As expected, assimilating ATMS data improves the 6-hour forecast fits to both channels. The ATMS_Tch experiment shows improvements across most latitudes, and the additional assimilation of humidity-sounding and window channels in ATMS_THSch further enhances performance. In the tropics, RMSE reductions exceed 2% for channel 4 and 1% for channel 15. Overall, the improved background fits to AMSU-A 52.8 GHz and 89.0 GHz observations indicate a better representation of clouds due to the all-sky ATMS assimilation.

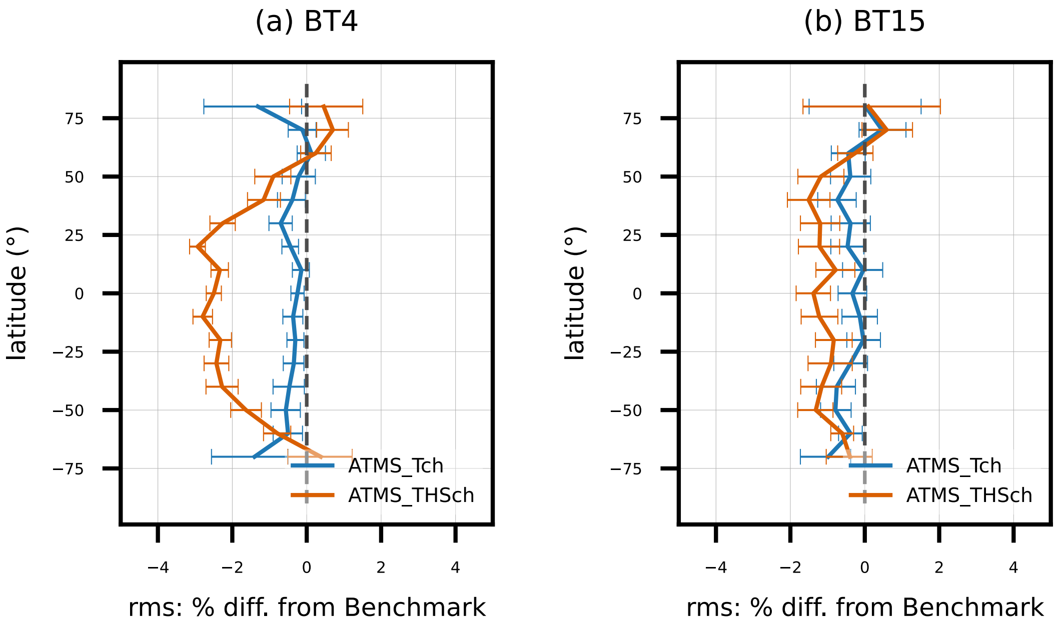

Figure 3 Relative RMSE difference of ATMS_Tch and ATMS_THSch with respect to RMSE of benchmark for METOP-A AMSU-A channel 4 52.8 GHz (a) and channel 15 89.0 GHz (b). Statistics are aggregated by latitude bins (every 10°) and over the period from 0000 UTC 18 April to 1800 UTC 14 May 2018. Error bars indicate 95% confidence intervals determined via bootstrap resampling.

Figure 4 shows the 6-hour forecast verification against brightness temperatures from the three water vapor channels of NOAA-18 MHS. The weighting function peaks for channels 3, 4, and 5 are approximately 300 hPa, 400 hPa, and 800 hPa, respectively. Among the three channels, the benchmark experiment exhibits large RMSEs over the Southern Ocean. In this region, the

ATMS_Tch experiment achieves RMSE reductions of approximately 4–9%. For channel 5, mixed results are observed in the tropics under ATMS_Tch. These improvements become more widespread and pronounced in the ATMS_THSch experiment, with RMSE reductions evident across nearly all regions and reaching up to ~18% in many areas.

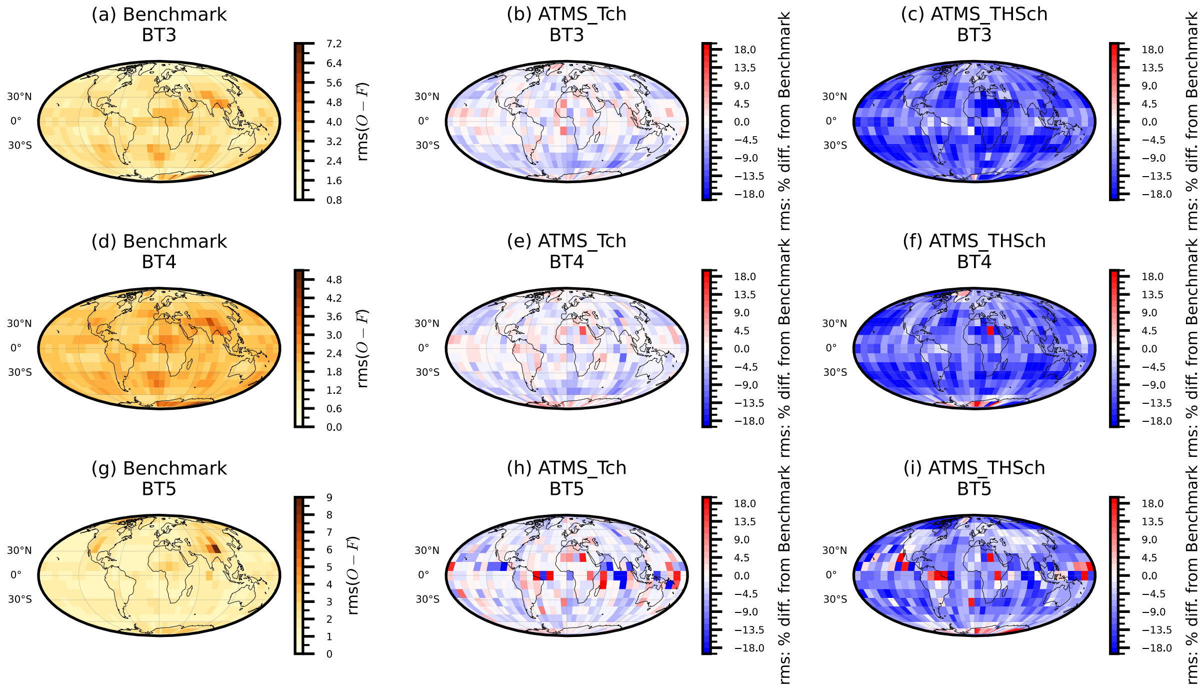

Figure 4 Left column: RMSE of 6-h forecast background from the benchmark with respect to NOAA-18 MHS channels 3-5 (a, d, g). Middle and right columns: relative RMSE change for ATMS_Tch and ATMS_THSch, respectively, with respect to the benchmark. Statistics are aggregated over the period from 0000 UTC 18 April to 1800 UTC 14 May 2018.

In addition to observation-space verification, model-space verification of the 6-hour forecasts against GFS analyses further demonstrates improvements from ATMS_Tch and ATMS_THSch relative to the benchmark (Fig. 5). The verification was conducted for T, water vapor mixing ratio (Qv), U, and V by comparing the 6-hour forecasts against GFS analyses. For temperature, improvements are primarily observed above model level 20 (~ 700 hPa), with RMSE reductions increasing with height and exceeding 6 % near the model top. An exception occurs near model level 40 (approximately the tropopause), where the improvement is less pronounced. Due to multivariate correlations in the assimilation system, assimilating temperature-sounding channels also benefits tropospheric Qv, resulting in an RMSE reduction of approximately 0.2 %. When additional humidity-sounding and window channels are assimilated in ATMS_THSch, Qv improvements become more substantial throughout the entire troposphere, with RMSE reductions of about 2%. Significant improvements in U and V (Figs. 5c and 5d) are also evident across all model levels in ATMS_Tch, with RMSE reductions of approximately 1% below level 20 and increasing to around 3% near the model top. These results are consistent with the observation-space verification presented in Figs. 2d–2i. For both ATMS_Tch and ATMS_THSch, the largest RMSE reductions (exceeding 4%) near the model top for T,

https://doi.org/10.5194/egusphere-2026-1047
Preprint. Discussion started: 6 March 2026

U, and V are primarily attributed to the temperature-sounding channels 9 and 10. Overall, both ATMS_Tch and ATMS_THSch demonstrate clear improvements over the benchmark, with notable RMSE reductions.

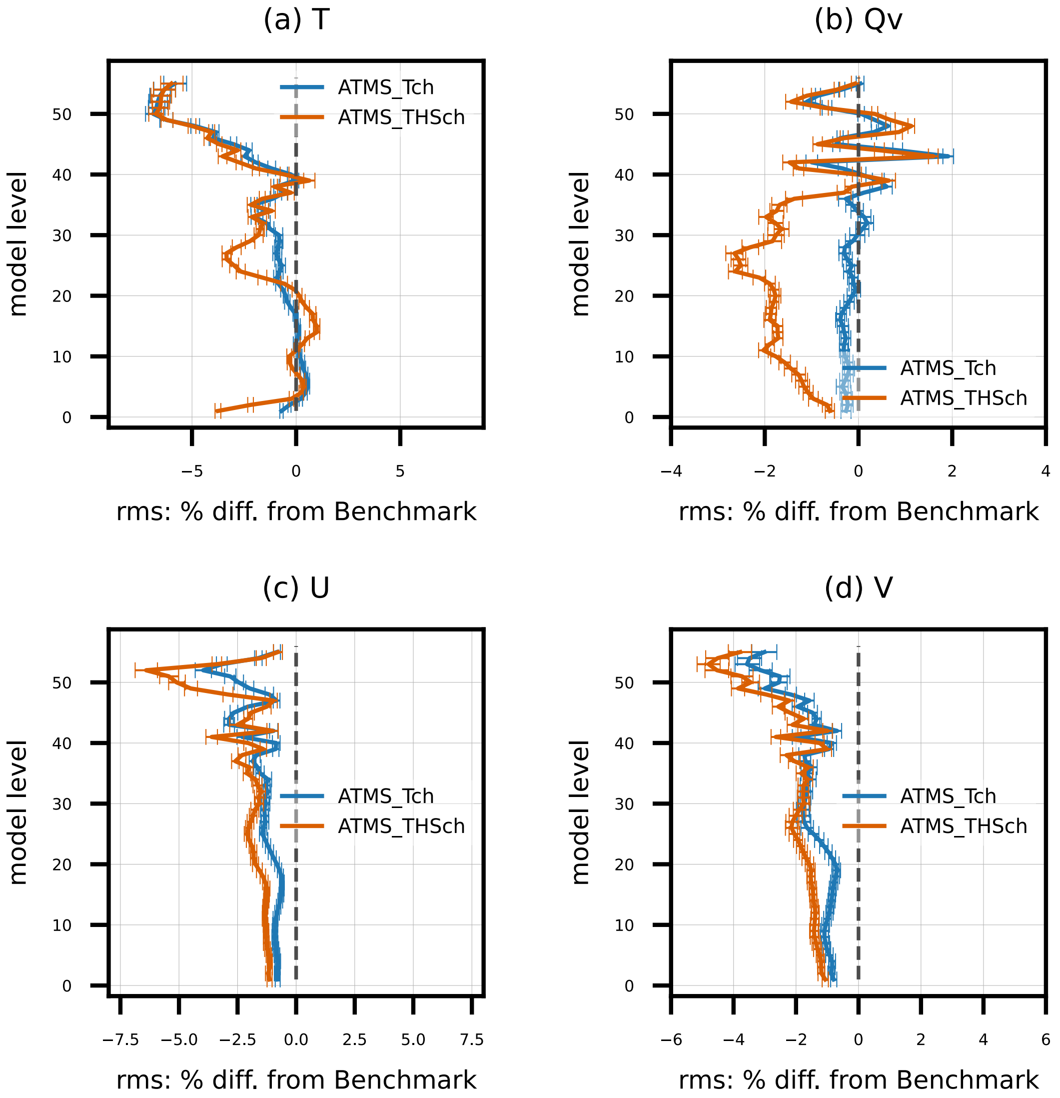

310 **Figure 5 Relative differences in RMSE of 6-h forecasts of T (a), Qv (b), U(c) and V(d) for ATMS_Tch and ATMS_THSch from benchmark. Statistics are aggregated over the period from 0000 UTC 18 April to 1800 UTC 14 May 2018. Error bars indicate 95% confidence intervals determined via bootstrap resampling.**

5.2 Extended forecast verification

5.2.1 Observation space verification

The impacts of all-sky ATMS radiance assimilation were demonstrated using 5-day forecasts, verified against independent ABI and GMI radiances using the MPAS-JEDI's HofX3D application. Before ingestion into MPAS-JEDI, the raw ABI infrared channel data at 2 km resolution undergo cloud detection at each pixel following Wu et al. (2020) and are preprocessed into super-observations averaged over 15 by 15 pixels.

Figure 6 shows the relative RMSE reductions as a function of forecast lead time for ABI water vapor channel 10 and window channel 13. Error statistics are aggregated over 27 forecasts initialized at 0000 UTC from 18 April to 14 May 2018. ABI channel 10 (7.3 µm) is sensitive to lower to mid-tropospheric moisture, while window channel 13 (10.4 µm) is sensitive to surface temperature and cloud-top temperature. For channel 10 (Fig. 6a), the RMSE reduction is fluctuated, ranging from 0.25% to 0.75% over most forecast lead times in the ATMS_Tch experiment. For channel 13 (Fig. 6b), the RMSE reduction becomes more pronounced at longer forecast ranges (day 4 and 5). This trend—improvements in longer-range forecasts—is particularly evident in the ATMS_THSch experiment.

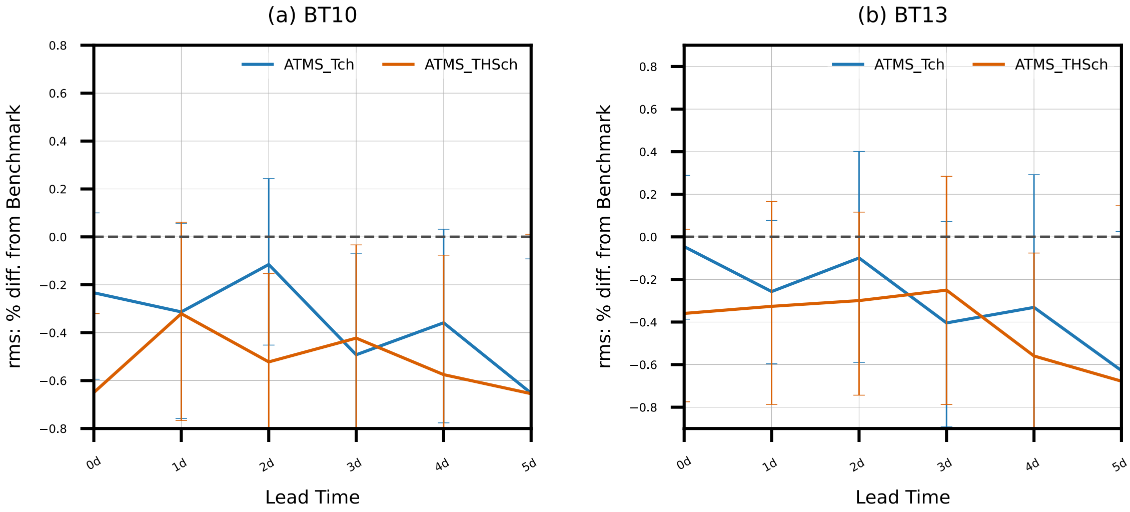

Figure 6 Relative RMSE reductions in ABI channels 10 (a) and 13 (b) brightness temperature space between ATMS_Tch, ATMS_THSch and benchmark as a function of forecast lead time. Error statistics are aggregated over 27 forecasts initialized at 0000 UTC from 18 April to 14 May 2018. Error bars indicate 95% confidence intervals determined via bootstrap resampling.

Figure 7 shows the relative RMSE differences verified against GMI channel 5 (23.5 GHz) over different regions as a function of forecast lead time. In the ATMS_Tch experiment, RMSE reductions are evident during the first three days over the Northern Extratropics (NX), with statistically significant improvements. Statistically significant improvements are also observed over the Southern Tropics (ST; 5°S–30°S) on days 2 and 3. In contrast, improvements over the Intertropical Convergence Zone

https://doi.org/10.5194/egusphere-2026-1047
Preprint. Discussion started: 6 March 2026

(ITCZ) are limited and not statistically significant. In the ATMS_THSch experiment, a maximum RMSE reduction of ~3% is observed at analysis time over the 30°S–30°N region, with statistically significant improvements maintained up to four days within the ITCZ.

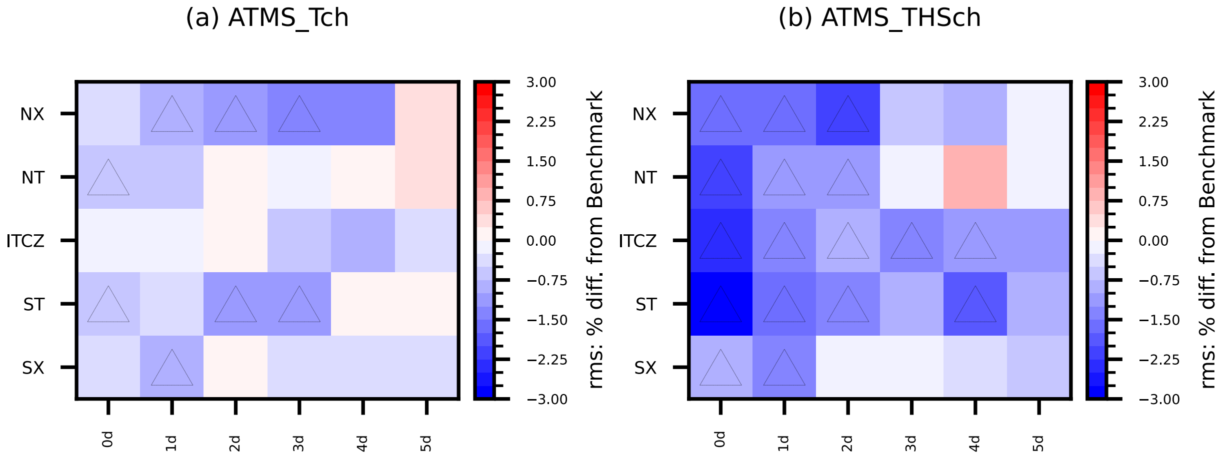

Figure 7 The relative difference in RMSE of between ATMS_Tch (a), ATMS_THSch (b) and benchmark as a function forecast lead time with respect to GMI channel 5 (23.5 GHz). Regions are defined as NX (northern extratropic; 30°N–90°N), NT (northern tropical; 5°N–30°N), ITCZ (intertropical convergence zone; 5°S–5°N), ST (southern tropical; 5°S–30°S), and SX (southern extratropic; 30°S–90°S). The upward (downward) black triangles indicate the statistically significant improvements (degradations) above the 95% confidence level.

5.2.2 Model space verification

Figure 8 shows the relative RMSE differences, verified against GFS analyses, for 500 hPa T, relative humidity (RH), and wind fields as a function of forecast lead time. For the ATMS_Tch experiment, the most notable improvements occur in the extratropical regions (NX and SX), consistent with the benefits observed from ATMS assimilation in the 6-hour forecast. These improvements persist for the first three forecast days and extend up to five days in NX and the tropics (TR). For the ATMS_THSch experiment, improvements are observed throughout the 5-day forecast, particularly for TR and SX. After assimilating humidity sounding channels and window channels, the improvements persist for a longer lead time. In Zhu et al. (2019), RMSE reduction for vector wind in the all-sky ATMS experiment over the Southern Hemisphere was also investigated, but the improvements were small and typically not statistically significant. This may be related to the fact that ATMS all-sky radiances are only used under non-precipitating conditions in Zhu et al. (2019). In contrast, this study includes the mixing ratios of five hydrometeors and assimilates ATMS radiances over both land and ocean for temperature and moisture channels.

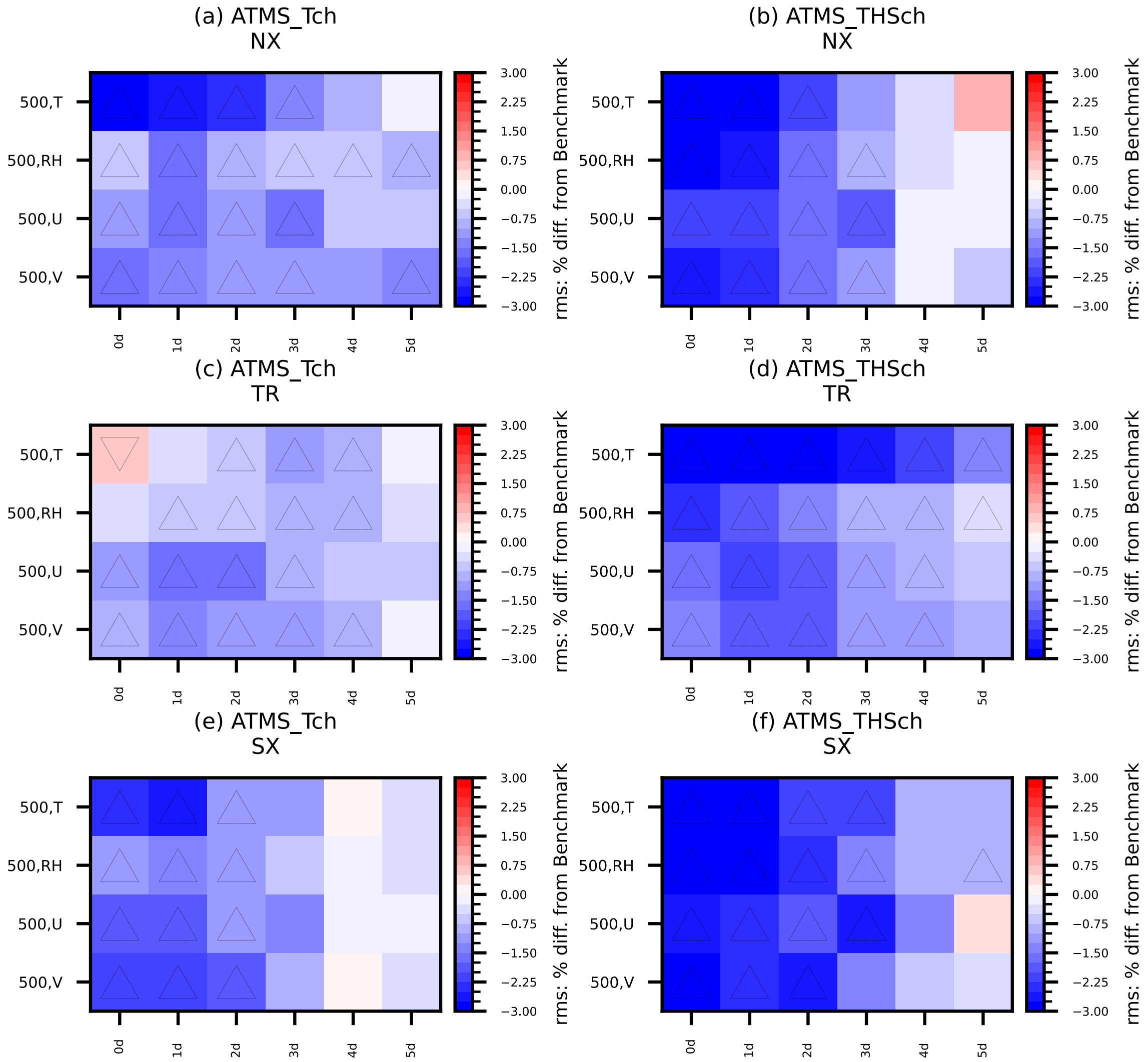

Figure 8 The relative RMSE difference in 500 hPa T, RH, U, and V between ATMS_Tch, ATMS_THSch and Benckmark as a function of forecast lead time for three regions, using GFS analyses as reference. The upward (downward) black triangles indicate the statistically significant improvements (degradations) above the 95% confidence level. NX (northern extratropic, 30°N~90°N), TR (tropical , -30°S~30°N), and SX (southern extratropic, -30°S~-90°S).

Figure 9 shows the relative RMSE differences with respect to GFS analyses between the two ATMS experiments and the benchmark for 0 to 5-day forecasts. The improvements in T for both experiments are very close with a 4% RMSE reduction at analysis time and decrease approximately 0.5% per day as lead time increases. It should be noted that these statistics are over all vertical levels and all grid points. For Qv, assimilation of ATMS temperature sounding channels results in approximately a 0.5% RMSE reduction for almost all lead times. The ATMS_THSch experiment further reduces RMSE by

0.5-1.5%, with improvements persisting through the 5-day forecast. For the wind fields, improvements are evident at the 5-day forecast in ATMS_Tch, and RMSE is further reduced in ATMS_THSch, especially for longer lead times. Overall, both ATMS_Tch and ATMS_THSch demonstrate consistent and encouraging forecast improvements relative to the Benchmark.

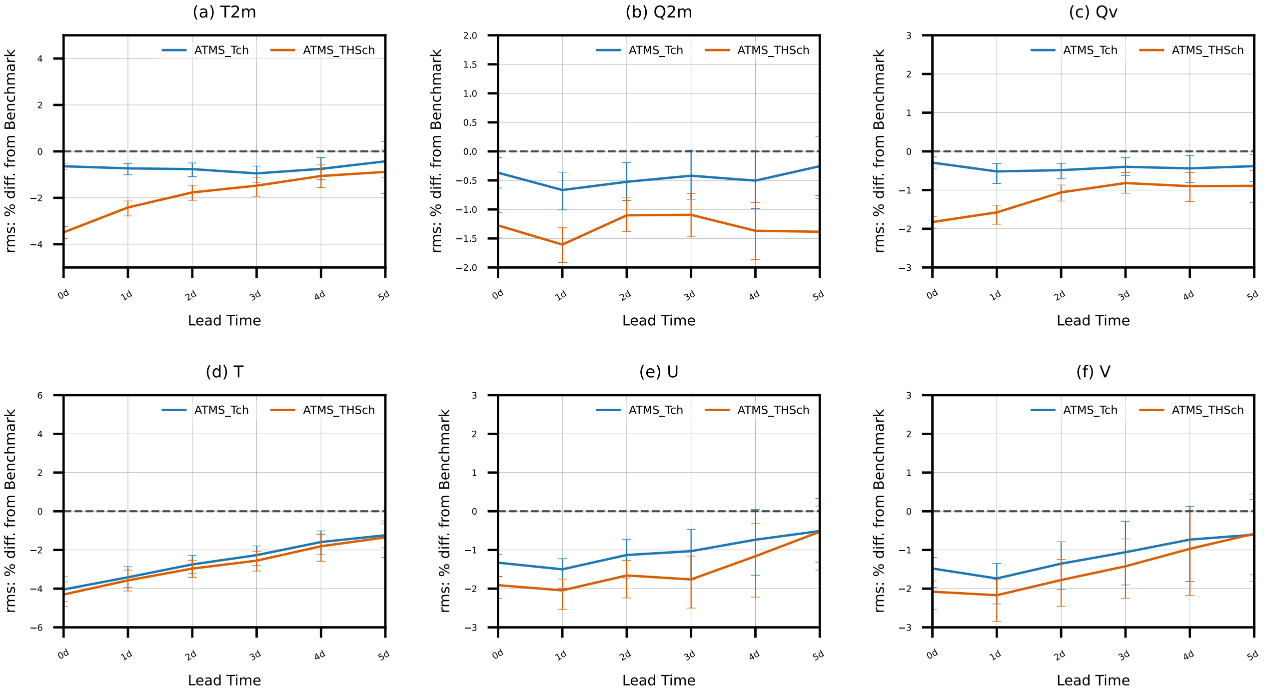

Figure 9 Relative RMSE (with respect to GFS analyses) differences as a function of forecast lead time (0-5-day) for T2m, Q2m, T, Qv, U, and V. Error statistics are over the globe and aggregated over 27 forecasts initialized at 0000 UTC from 18 April to 14 May 2018. RMSE differences are between experiments ATMS_Tch, ATMS_THSch and the benchmark experiment.

6 Conclusions

In this study, the assimilation of all-sky radiances in MPAS-JEDI has been extended to include ATMS observations. Compared to the previously implemented AMSU-A all-sky assimilation, ATMS covers a broader frequency range from 23.8 GHz to 183 GHz. In Liu et al. (2022), AMSU-A temperature sounding channels were assimilated under clear-sky conditions. In this study, ATMS temperature sounding channels are assimilated under all-sky conditions (experiment ATMS_Tch). Because both window channels and humidity sounding channels influence the moisture fields, these channels are assimilated together with temperature-sensitive channels in the ATMS_THSch experiment. Three month-long hybrid-3DEnVar experiments were conducted to evaluate the impact of assimilating all-sky ATMS radiances, in comparison with a benchmark experiment that assimilates conventional observations, clear-sky (all-sky) radiances from AMSU-A temperature-sounding (window) channels, and MHS water vapor channels.

Including all-sky temperature sounding channels (ATMS_Tch) improved the 6-hour forecast background fits to radiosonde observations, satellite radiances, and GFS analyses. The improvements in humidity and wind fields in ATMS_Tch can be attributed to multivariate correlations within the assimilation system. Additional benefits are obtained in the ATMS_THSch experiment, particularly for the moisture field, as expected. Verification of 5-day forecasts against independent ABI radiances and GFS analyses shows sustained improvements: ATMS_Tch enhances forecasts up to 4 days, while ATMS_THSch yields further gains, especially at longer lead times. Overall, both experiments demonstrate consistent and encouraging improvements across dynamical, thermodynamic, and moisture-related fields.

In the future, further enhancements can be made for ATMS all-sky radiance assimilation in MPAS-JEDI. First, the inter-channel error correlations, which have been shown to be important in clear-sky ATMS assimilation, could also be considered for all-sky DA. Bormann et al. (2013) highlighted significant inter-channel correlations for SNPP ATMS channels 18–22, while Weston and Bormann (2018) reported reduced correlation levels for NOAA-20 ATMS compared to SNPP ATMS. Secondly, developing a VarBC scheme tailored specifically for all-sky DA would likely further improve performance and should be explored in future studies. Moreover, the current observation error model is based on globally averaged statistics. Previous studies (Weston et al., 2019; Duncan et al., 2022a) have shown that such global error models behave differently across latitudes—overweighting observation errors in the tropics (Weston et al., 2019) and underweighting them in the extratropics (Duncan et al., 2022a). Therefore, investigating a situation-dependent error model that accounts for latitudinal variations could lead to more optimal use of all-sky radiance data.

Code and data availability

The source code of MPAS-JEDI 2.1.0 is available on Zenodo at https://doi.org/10.5281/zenodo.15201032 (last access: 23 February 2026; Joint Center for Satellite Data Assimilation and National Center for Atmospheric Research, 2023). Global Forecast System analyses are available from NCAR Research Data Archive (RDA) https://rda.ucar.edu/datasets/ds084.1/ (last access: 23 February 2026; National Centers For Environmental Prediction/National Weather Service/NOAA/U.S. Department Of Commerce, 2015). Global Ensemble Forecast System ensemble analyses are downloaded from https://www.ncei.noaa.gov/products/weather-climate-models/global-ensemble-forecast (last access: 23 February 2026). Conventional and satellite observations assimilated are downloaded from NCAR RDA https://rda.ucar.edu/datasets/d337000 (last access: 23 February 2026; National Centers For Environmental Prediction/National Weather Service/NOAA/U.S. Department Of Commerce, 2008) and https://rda.ucar.edu/datasets/d735000/ (last access: 23 February 2026; National Centers For Environmental Prediction/National Weather Service/NOAA/U.S. Department Of Commerce, 2009). ATMS radiance data are downloaded from https://sounder.gesdisc.eosdis.nasa.gov/opendap (last access: 23 February 2026).

Author contributions

JB designed, conducted, and analysed all experiments and wrote the manuscript. ZL aided with experimental design and analysis. All co-authors contributed to the development of the MPAS-JEDI, preparation of externally sourced data, design of experiments, and preparation of the manuscript.

Competing interests

The authors have no competing interests.

Acknowledgements

The National Center for Atmospheric Research (NCAR) is sponsored by the National Science Foundation of the United States. The numerical calculations of this study are supported by NCAR's Computational and Information Systems Laboratory (CISL).

Financial support

This research has been supported by the United States Air Force (grant no. NA21OAR4310383).

References

Bauer, P., Geer, A. J., Lopez, P., and Salmond, D.: Direct 4D-Var assimilation of all-sky radiances. Part I: Implementation, Q. J. Roy. Meteor. Soc., 136, 1868–1885, 2010.

Bauer P., Moreau E., Chevallier F. and O'Keeffe U.: Multiple-scattering microwave radiative transfer for data assimilation applications. Q. J. Roy. Meteor. Soc., 132, 1259–1281, 2006.

Bormann, N., A. Fouilloux, and William, B.: Evaluation and assimilation of ATMS data in the ECMWF system, ECMWF Technical Memoranda No. 689, 1-41, 2013

Bormann, N., Geer, A., and English, S.: Evaluation of the microwave ocean surface emissivity model FASTEM-5 in the IFS, ECMWF Reading, UK, 2012.

Candy, B. and Migliorini, S.: The assimilation of microwave humidity sounder observations in all-sky conditions, Q. J. Roy. Meteor. Soc., 147, 3049–3066, 2021.

Draper, D. W., Newell, D. A., Wentz, F. J., Krimchansky, S., and Skofronick-Jackson, G. M.: The global precipitation measurement (GPM) microwave imager (GMI): Instrument overview and early on-orbit performance, IEEE Journal of Selected Topics in Applied Earth Observations and Remote Sensing, 8, 3452–3462, 2015.

Duncan, D., Bormann, N., and Geer, A.: All-sky assimilation of AMSU-A window channels, EUMETSAT/ECMWF Fellowship Programme Research Report, 59, 34, 2022a.

Duncan, D. I., Bormann, N., Geer, A. J., and Weston, P.: Assimilation of AMSU-A in all-sky conditions, Mon. Wea. Rev., 150, 1023–1041, 2022b.

English, S. J. and Hewison, T. J.: Fast generic millimeter-wave emissivity model, in: Microwave remote sensing of the atmosphere and environment, vol. 3503, pp. 288–300, SPIE, 1998.

Geer, A., Baordo, F., Bormann, N., Chambon, P., English, S., Kazumori, M., Lawrence, H., Lean, P., Lonitz, K., and Lupu, C.: The growing impact of satellite observations sensitive to humidity, cloud and precipitation, Q. J. Roy. Meteor. Soc., 143, 3189–3206, 2017.

Geer, A. J., and Bauer, P.: Observation errors in all-sky data assimilation, Q. J. Roy. Meteor. Soc., 137, 2024– 2037, 2011.

Geer, A. J., Bauer, P., and Lopez, P.: Direct 4D-Var assimilation of all-sky radiances. Part II: Assessment, Q. J. Roy. Meteor. Soc., 136, 1886–1905, 2010.

Geer, A. J., Bauer, P. and O'Dell, C. W.: A revised cloud overlap scheme for fast microwave radiative transfer in rain and cloud. J. Appl. Meteorol. and Climatol., doi:10.1175/2009JAMC2170.1, 2009.

Geer, A. J., Bauer, P., and English, S. J.: Assimilating AMSU-A temperature sounding channels in the presence of cloud and precipitation, ECMWF Reading, UK, 2012.

Geer, A. J., Fabrizio, B., Bormann, N., and English, S.: All-sky assimilation of microwave humidity sounders, Reading: ECMWF. ECMWF Technical Memorandum, Vol. 741, 2014.

Geer, A. J., Lonitz, K., Weston, P., Kazumori, M., Okamoto, K., Zhu, Y., Liu, E. H., Collard, A., Bell, W., Migliorini, S., et al.: All-sky satellite data assimilation at operational weather forecasting centres, Q. J. Roy. Meteor. Soc., 144, 1191– 1217, 2018.

Grody, N., Zhao, J., Ferraro, R., Weng, F., and Boers, R.: Determination of precipitable water and cloud liquid water over oceans from the NOAA 15 advanced microwave sounding unit, Journal of Geophysical Research: Atmospheres, 106, 2943–2953, 2001.

Guerrette, J. J., Liu, Z., Snyder, C., Jung, B.-J., Schwartz, C. S., Ban, J., Vahl, S., Wu, Y., Baños, I. H., Yu, Y. G., Ha, S., Trémolet, Y., Auligné, T., Gas, C., Ménétrier, B., Shlyaeva, 415 A., Miesch, M., Herbener, S., Liu, E., Holdaway, D., and Johnson, B. T.: Data assimilation for the Model for Prediction Across Scales – Atmosphere with the Joint Effort for Data assimilation Integration (JEDI-MPAS 2.0.0-beta): ensemble of 3D ensemble-variational (En-3DEnVar) assimilations, Geosci. Model Dev., 16, 7123–7142, https://doi.org/10.5194/gmd-16-7123-2023, 2023.

Han, Y., van Delst, P., Liu, Q., Weng, F., Yan, B., Treadon, R., and Derber, J.: JCSDA Community Radiative Transfer Model (CRTM) – Version 1, NOAA Tech. Rep. NESDIS 122, 33 pp., NOAA, Silver Spring, Md, USA, 2006.

Hong, S.-Y. and Lim, J.-O. J.: The WRF Single-Moment 6-Class Microphysics Scheme (WSM6), J. Korean Meteor. Soc., 42, 129–151, 2006.

Joint Center for Satellite Data Assimilation and National Center for Atmospheric Research: JEDI-MPAS Data Assimilation System v2.1.0 (2.1.0), Zenodo [code], https://doi.org/10.5281/zenodo.15201032, 2023.

Jung, B.-J., Ménétrier, B., Snyder, C., Liu, Z., Guerrette, J. J., Ban, J., Baños, I. H., Yu, Y. G., and Skamarock, W. C.: Three-dimensional variational assimilation with a multivariate background error covariance for the Model for Prediction Across Scales – Atmosphere with the Joint Effort for Data assimilation Integration (JEDI-MPAS 2.0.0-beta), Geosci. Model Dev., 17, 3879–3895, https://doi.org/10.5194/gmd-17-3879-2024, 2024.

Kazumori, M. and English, S. J.: Use of the ocean surface wind direction signal in microwave radiance assimilation, Q. J. Roy. Meteor. Soc., 141, 1354–1375, 2015.

Kazumori, M. and Kadowaki, T.: Development of an all-sky assimilation of microwave imager and sounder radiances for the Japan Meteorological Agency global numerical weather prediction system, in: Proceedings for the 21st International TOVS Study Conference, vol. 20, 2017.

Kazumori, M., Geer, A. J., and English, S. J.: Effects of all-sky assimilation of GCOM-W/AMSR2 radiances in the ECMWF numerical weather prediction system, Q. J. Roy. Meteor. Soc., 142, 721–737, 2016.

Lawrence, H., Bormann, N., Geer, A. J., Lu, Q., and English, S. J.: Evaluation and assimilation of the microwave sounder MWHS-2 onboard FY-3C in the ECMWF numerical weather prediction system, IEEE Trans. Geosci. Remote Sens., 56, 3333–3349, 2018.

Liu, Q. and Weng, F.: Advanced doubling–adding method for radiative transfer in planetary atmospheres, J. Atmos. Sci., 63, 3459–3465, 2006.

Liu, Q., Weng, F., and English, S. J.: An improved fast microwave water emissivity model, IEEE Trans. Geosci. Remote Sens., 49, 1238–1250, 2010.

Liu, Z., Snyder, C., Guerrette, J. J., Jung, B.-J., Ban, J., Vahl, S., Wu, Y., Trémolet, Y., Auligné, T., Ménétrier, B., B., Shlyaeva, A., Herbener, S., Liu, E., Holdaway, D., and Johnson, B. T.: Data assimilation for the Model for Prediction Across Scales–Atmosphere with the Joint Effort for Data assimilation Integration (JEDI-MPAS 1.0. 0): EnVar implementation and evaluation, Geosci. Model Dev., 15, 7859–7878, https://doi.org/10.5194/gmd-15-7859-2022, 2022.

Migliorini, S. and Candy, B.: All-sky satellite data assimilation of microwave temperature sounding channels at the Met Office, Q. J. Roy. Meteor. Soc., 145, 867–883, 2019.

Murata, H. and Kamekawa, N.: Operational Use of NOAA-20 ATMS and CrIS Radiance Data in JMA's Global NWP System.

Nystrom, R. G., Snyder, C., Liu, Z., Jung, B-J., Ban, J., and Baños, I. H.: A hybrid four-dimensional variational data assimilation system for the Model for Prediction Across Scales (MPAS-atmosphere): Leveraging the Joint Effort for Data assimilation Integration (JEDI). Journal of Advances in Modeling Earth Systems, 17(12), e2025MS005183, 2025.

Skamarock, W. C., Klemp, J. B., Duda, M. G., Fowler, L. D., Park, S.-H., and Ringler, T. D.: A multiscale nonhydrostatic atmospheric model using centroidal Voronoi tesselations and C-grid staggering, Mon. Wea. Rev., 140, 3090–3105, 2012.

Skamarock, W. C., Duda, M. G., Ha, S., and Park, S.-H.: Limited-area atmospheric modeling using an unstructured mesh, Mon. Wea. Rev., 146, 3445–3460, 2018.

Tong, M., Zhu, Y., Zhou, L., Liu, E., Chen, M., Liu, Q., and Lin, S.-J.: Multiple hydrometeors all-sky microwave radiance assimilation in FV3GFS, Mon. Wea. Rev., 148, 2971–2995, 2020.

Sun, T., Guerrette, J. J., Liu, Z., Ban, J., Jung, B.-J., Baños, I. H., and Snyder, C.: All-sky AMSU-A radiance data assimilation using the gain-form of Local Ensemble Transform Kalman filter within MPAS-JEDI-2.1.0: implementation, tuning, and evaluation, Geosci. Model Dev., 18, 8569–8587, https://doi.org/10.5194/gmd-18-8569-2025, 2025.

Trémolet, Y. and Auligné, T.: The Joint effort for data assimilation integration (JEDI), JCSDA Q, 66, 1–5, 2020.

Weston, P. and Bormann, N.: Enhancements to the Assimilation of ATMS at ECMWF: Observation Error Update and Addition of NOAA-20; EUMETSAT, Tech. rep., ECMWF Fellowship Programme Research Report, 2018.

Weng, F., Zou, X., Sun, N., Yang, H., Tian, M., Blackwell, W.J., Wang, X., Lin, L. and Anderson, K.: Calibration of Suomi national polar-orbiting partnership advanced technology microwave sounder. J. Geophys. Res.-Atmos., 118(19), 11-187, 2013

Weston, P., A. J. Geer, and Bormann N.: Investigations into the assimilation of AMSU-A in the presence of cloud and precipitation. EUMETSAT/ECMWF Tech. Rep. 50, 42 pp., https://doi.org/10.21957/ewahn9ce, 2019.

Wu, Y., Liu, Z., and Li, D.: Improving forecasts of a recordbreaking rainstorm in Guangzhou by assimilating every 10-min AHI radiances with WRF 4DVAR, Atmos. Res., 239, 104912, https://doi.org/10.1016/j.atmosres.2020.104912, 2020.

Zhao, Q., and F. H. Carr: A prognostic cloud scheme for operational NWP models. Mon. Wea. Rev., 125, 1931–1953, 1997.

Zhu, Y., Derber, J., Collard, A., Dee, D., Treadon, R., Gayno, G., and Jung, J. A.: Enhanced radiance bias correction in the National Centers for Environmental Prediction's Gridpoint Statistical Interpolation data assimilation system, Q. J. Roy. Meteor. Soc., 140, 1479–1492, 2014.

Zhu, Y., Liu, E., Mahajan, R., Thomas, C., Groff, D., Van Delst, P., Collard, A., Kleist, D., Treadon, R., and Derber, J. C.: All-sky microwave radiance assimilation in NCEP's GSI analysis system, Mon. Wea. Rev., 144, 4709–4735, 2016.

Zhu, Y., Gayno, G., Purser, R. J., Su, X., and Yang, R.: Expansion of the all-sky radiance assimilation to ATMS at NCEP, Mon. Wea. Rev., 147, 2603–2620, 2019.